Preparation and Characterization of a Novel Triple Composite Scaffold Containing Silk Fiborin, Chitosan, and Alginate for 3D Culture of Colonic Carcinoma Cells *In Vitro*

Authors' Contribution:
Study Design A
Data Collection B
Statistical Analysis C
Data Interpretation D
Manuscript Preparation E
Literature Search F
Funds Collection G

ACF Xianhao Su*
AD Liang Chen*
B Shanliang Han
F Gengming Niu
C Jun Ren
AG Chongwei Ke

Department of General Surgery, Fifth People's Hospital of Shanghai, Fudan University, Shanghai, P.R. China

Corresponding Author: * Xianhao Su and Liang Chen contributed equally
Chongwei Ke, e-mail: Shchweiz@126.com

Background: Three-dimensional (3D) cell-culture scaffolds are ideal *in vitro* models to bridge the gap between two-dimensional cell culture *in vitro* and *in vivo* cancer models. Construction of 3D scaffolds using two kinds of biomaterials has been reported, but there are still many defects. To improve the performance of the scaffolds for 3D cell culture of colonic carcinoma (CC) cells *in vitro*, we attempted to construct triple composite scaffolds using silk fibroin (SF), chitosan (Cs), and alginate (Alg).

Material/Methods: We explored the suitability of triple composite scaffolds of SF/Cs/Alg at ratios of 1: 1: 0.5, 1: 1: 1, and 1: 1: 2 for 3D culture of CC cells, and used the dual composite scaffold of SF/Cs (1: 1) as a control group. We analyzed the physicochemical characteristics of these scaffolds and studied cell adhesion, cell proliferation, migration, colony-forming ability, microstructure and ultrastructure, and spheroid-forming capacity of the commercially available CC cell line HCT-116 on the prepared scaffolds.

Results: Our results show that SF/Cs/Alg (1: 1: 1) scaffolds demonstrated the best profile, the highest uniform porosity and connectivity, and excellent hydroscopicity, and also exhibited appropriate and controlled swelling and degradation characteristics. The adhesion, proliferation, colony-forming, and wound-healing assays, green fluorescent protein-labeled HCT116 cell imaging, 4',6-diamidino-2-phenylindole and DY-554-phalloidin staining, scanning electron microscopy, and haematoxylin and eosin staining revealed that the triple composite scaffolds of SF/CS/Alg (1: 1: 1) supported cell adhesion, proliferation, migration, colony-forming ability, and spheroid formation far better than the dual composite scaffold of SF/CS (1: 1).

Conclusions: This study successfully demonstrated the potential of SF/Cs/Alg (1: 1: 1) scaffold as an alternative for the 3D *in vitro* culture of CC cells.

MeSH Keywords: Alginates • Chitosan • Colorectal Neoplasms, Hereditary Nonpolyposis • Fibroins • Tissue Scaffolds

Full-text PDF: https://www.medscimonit.com/abstract/index/idArt/922935

📄 5917   📊 1   📈 10   📚 36

Background

Colonic carcinoma (CC) is the world's second-deadliest malignancy after lung cancer, with almost 881 000 deaths every year [1]. The disease can be considered a marker of socioeconomic development, as the highest rates of incidence are in developed countries [2]. As more people become richer and adopt the Western diet and lifestyle, the incidence of CC is likely to increase. The classical two-dimensional (2D) cell culture provides researchers a convenient *in vitro* platform for CC research. However, cells cultured on flat Petri dish surfaces exhibit a dramatically reduced malignant phenotype and do not represent the true cell-extracellular matrix (ECM) and cell–cell interactions or architecture of tumors *in vivo* [3]. This discrepancy may lead to the wrong prediction of the biological behavior of cancers. Hence, there is an urgent need for the development of ideal *in vitro* experimental models for CC that would allow researchers to conduct reliable experiments *in vitro* in a more controlled environment.

The scientific literature has demonstrated that three-dimensional (3D) cell culture systems are ideal *in vitro* models to bridge the gap between the *in vitro* and *in vivo* cancer models and help to reduce the loss of animal life, defray costs, and shorten the experiment time [4,5]. In tumors, cells maintain close contact with each other. Cells cultured in a 3D system replicate the architecture, phenotype, and malignancy of tumors *in vivo*. Moreover, 3D tumor models can unravel the complex interactions observed in tumor tissues *in vivo*, such as metabolic reprogramming and oxygen gradient [6]. The production of a scaffold with adequate pore size and porosity, good water-binding ability, high affinity, along with good biocompatibility and biodegradability, is crucial for developing a successful 3D tumor model. There are a variety of methods to fabricate such scaffolds, including gas foaming [7], particulate leaching [8], electrospinning [9], and freeze drying [10]. To produce scaffolds, natural biomaterials such as collagen, gelatin, and the commercially available matrigel have been used. However, these animal-derived products are expensive, immunogenic, and can potentially transmit pathogens [11]. Synthetic polymers such as polyurethane, polylactide-co-glycolide, and polyacrylonitrile have also been studied, but they can release acidic byproducts that are toxic to cells [12]. Silk fibroin (SF) has been used as a potential biomaterial because of its excellent biological compatibility, lower cost, and reduced immunogenicity. The spongelike SF scaffold fabricated by the freeze-drying method has shown high oxygen and adequate water permeability. However, the spongelike SF scaffold is brittle and crispy and has a sheetlike structure, thereby limiting its application in 3D cell culture [13]. Chitosan (Cs), a natural polymer derived from nonanimal sources, has many inherent advantages in terms of immunogenicity and biocompatibility, thereby making it suitable for development in a scaffold material.

Cs has been reported as a beneficial hemostatic agent for wound healing and osteoconduction because of its nontoxicity and enzymatic degradability [14]. However, the high swelling behavior of the Cs scaffold makes it prone to easy deformation. Hence, a scaffold made of pure Cs needs to be improved and optimized for practical applications. Alginate (Alg), another nonanimal-sourced natural polymer, is one of the potential materials used for the fabrication of polymeric scaffolds because of its excellent biocompatibility and the possibility to shape Alg hydrogel into a variety of sophisticated geometries and topologies [15]. However, the high degradation and swelling rate of the spongelike Alg scaffold limits its application as a kind of carrier for 3D cell culture.

To overcome the shortcomings of the scaffolds made exclusively from a single polymer, researchers have been exploring a composite system that includes more than one polymer. Multiple polymers in combination are expected to impart their individual properties and result in a scaffold that might facilitate cell adhesion, proliferation, and differentiation [16]. To date, SF/Cs (1: 1) scaffolds have been studied in sciatic nerve gap repair [17], cartilage repair [18], and reconstruction of bone defects [19]. Further, Cs/Alg scaffolds have been shown to provide an ideal growth environment for cartilage and bone regeneration [20] and stem cell renewal [21]. There are few reports on triple composite scaffolds in the literature, especially those using SF, Cs, and Alg as raw materials.

In this paper, a novel study on *in vitro* 3D cell culture of CC using SF/Cs/Alg scaffolds is presented. First, we explored the fabrication of a composite scaffold based on a SF/Cs/Alg polymer system (Figure 1). Then a neotype 3D tumor cell culture system was developed *in vitro* by seeding HCT-116 human colon adenocarcinoma cells on SF/Cs/Alg scaffolds (Figure 2).

Material and Methods

Material and animals

Cocoons of *Bombyx mori* (silkworm) were procured from farmers in Xuzhou, Jiangsu. Cs powders (900 000 Da, 95% deacetylated) were purchased from Shanghai Macklin Biochemical Technology Co. Ltd. Alg, sodium carbonate, lithium bromide, acetic acid, aqueous ethanol, polyethylene glycol 6000, dimethyl sulfoxide, cell counting kit (CCK)-8, 4% paraformaldehyde, hematoxylin, eosin, crystal violet, and dialysis bags were obtained from Shanghai Yuanye Biotechnology Co. Ltd. Ethylene dichloride (EDC) and *N*-hydroxysuccinimide (NHS) were bought from Sangon Biotech (Shanghai) Co. Ltd. Minimum essential medium culture media, fetal bovine serum, and penicillin–streptomycin were bought from Thermo Fisher Scientific Inc. (Waltham, MA). Four-week-old female BALB/c-nu mice were purchased
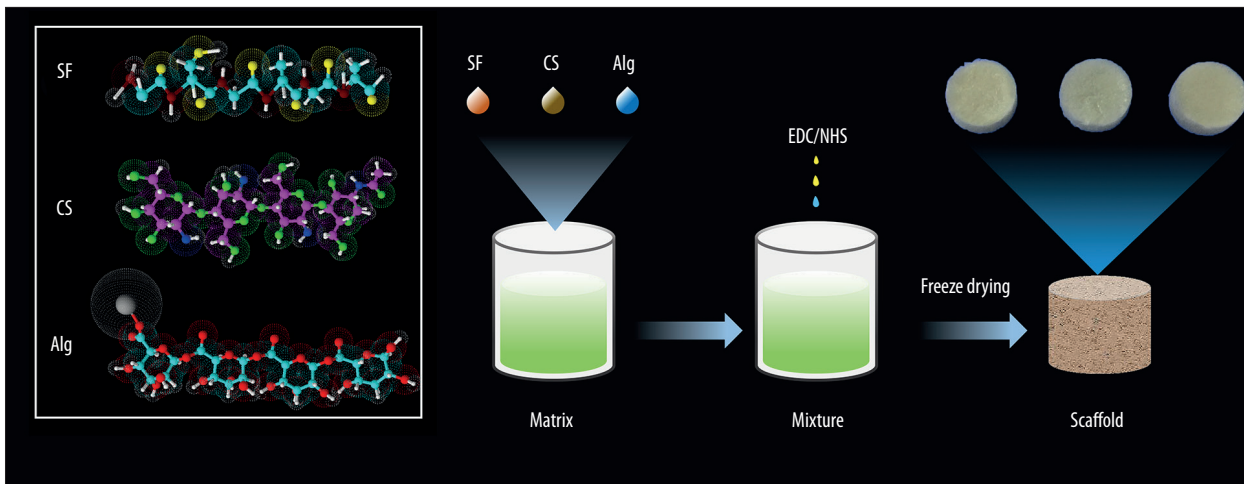
Figure 1. Schematic illustration of constructing a porous scaffold based on silk fibroin, chitosan, and alginate via freeze-drying technique and chemical cross-linking method.
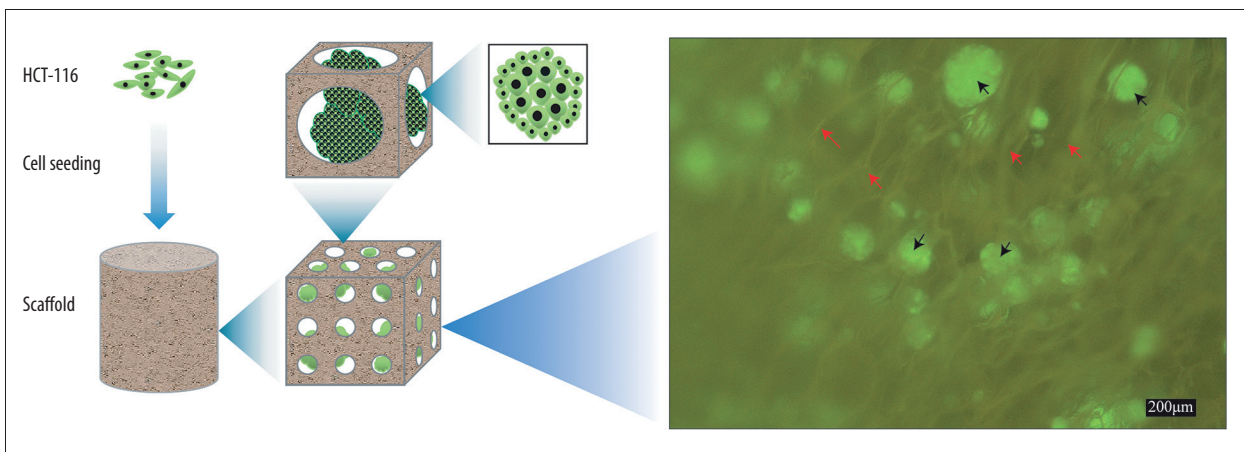

Figure 2. Schematic illustration of cells seeded on the scaffold to form biomaterial substrate-mediated multicellular spheroids. Red arrows represent the scaffold. Black arrows indicate the multicellular spheroids.

from the Animal Center of East China Normal University. Mice were bred and maintained under specific-pathogen-free conditions. The study was approved by the Hospital Ethical Committee (2019 JS-004, Shanghai Fifth People's Hospital), and all methods used in this study were carried out following the Regulations for the Administration of Affairs Concerning Experimental Animals approved by the State Council of the People's Republic of China. Commercially available human CC cells HCT-116 (1×10^7 cells/0.1 mL per site) were injected subcutaneously in the left underarm and right inguinal area of mice.

Scaffold synthesis and block design

The scaffolds for the experiments were produced via the freeze-drying technique and chemical cross-linking method reported previously [10]. Briefly, SF scaffolds were produced with 3% SF solution alone, Cs scaffolds were fabricated with 3% Cs solution alone, and Alg scaffolds were constructed with a pure 3% Alg solution. SF/Cs (1: 1) scaffolds were synthesized with a 1: 1 ratio (w/w) of SF solution and Cs solution. SF/Cs/Alg scaffolds were produced with different ratios of 1: 1: 0.5, 1: 1: 1, and 1: 1: 2 (w/w). Subsequently, 95% aqueous ethanol solution containing 50 mmol/L EDC and 18 mmol/L NHS were added to the mixtures with continuous magnetic stirring for 15 min to obtain a homogeneous solution. Next, the solution was added to wells of 24- and 96-well plates and left to cross-link at 4°C for 24 h. Subsequently, the samples were frozen at −20°C for 12 h before being placed in a −80°C freezer for another 12 h. The samples were maintained in a freeze-drying machine for 24 h to produce the scaffolds. Before initiating the cell culture, the scaffolds were sterilized with Cobalt 60 radiation for 72 h.

Characterization of the scaffolds

Macroscopic appearance

The 3D scaffolds were removed from the matrix (24-well plate) and compared using anterior-, posterior-, and lateral-view photography.

Internal morphology

The scaffolds were removed from the 24-well plates. The thin membrane with cross-sectional structure of the scaffold was left at the bottom of the well, and the structure of the thin membrane was viewed with an inverted microscope and photographed. Scanning electron microscopy (SEM, Hitachi, Washington, D.C.; S-3400N, serial no. 341352-08, accelerating voltage 10 000 V, working distance=6600 μm) was used to detect the surface morphology of the scaffold prepared. We cut the scaffold into thin slices with a surgical blade, stuck the slices on the sample table with conductive adhesive, used gold plate under vacuum for 20 s, observed the internal structure of the gold coating the scaffold and pore size distribution under SEM, and took pictures (5 images for each group, 100 pores per image for pore size measurement).

Porosity evaluation

As previously reported, the porosity of the scaffolds was measured by the liquid-displacement method described previously [22]. Briefly, the scaffolds were immersed in absolute ethanol until they were saturated, and they were weighed before and after immersion in alcohol. The porosity was calculated using the equation:

$$Porosity\ (\%) = (W_2 - W_1)/pV_1 \times 100\%,$$

where W_1 and W_2 indicate the weights of the scaffolds before and after immersion in alcohol, respectively; V_1 represents the volume of the scaffold before immersion in alcohol; and p is a constant (the density of alcohol).

Water absorption rate

Water absorption rate (%) was calculated as per the equation:

$$Water\ absorption\ rate\ (\%) = (W_2 - W_1)/W_1 \times 100\%,$$

where W_1 is the weight of the dry scaffold and W_2 is the weight of the scaffold after it is fully impregnated with water for 12 h at 37°C, with the excess surface water removed with filter paper.

Swelling rate

According to the change of the volume of the scaffolds in phosphate-buffered saline (PBS), the swelling rate (%) was obtained. The swelling rate was calculated as per the equation:

$$Sweeling\ rate\ (\%) = (V_2 - V_1)/V_1 \times 100\%,$$

where V_1 is the volume of prepared scaffolds ($V_1 = \pi d^2/4$; d is the cross-section diameter of the scaffold; h is the height). The dried scaffolds were placed in prepared PBS for 24 h at 37°C and the volume of the soaked scaffolds was taken as V_2.

Degradation property

The degradation ratio (%) was calculated as per the equation:

$$Degradation\ ratio\ (\%) = (W_0 - W_n)/W_0 \times 100\%,$$

where W_0 is the weight of the scaffolds before placing them in the culture medium in a 6-well plate in a humidified incubator at 37°C. Subsequently, the scaffolds were dried for 8 h at 60°C and weighed at 1, 3, 7, and 10 d (Wn).

Cell incorporation into scaffolds

Scaffolds were dampened with culture media and a total of 50 000cells in 50 μL of complete media was seeded onto them. The scaffolds were placed in 24-well plates and shaken on a vibrator for 5 min to settle the cells on the scaffold. Cells were allowed to infiltrate the scaffold in an incubator for 1 h, followed by the addition of 1 mL of fully supplemented media to each well. For samples precultured on 2D matrix, 50 000 cells in 1 mL of fully supplemented media were added to 24-well plate wells. The culture medium was replaced every other day.

Cell adhesion in scaffolds

Adhesion rate (%) was calculated as per the formula:

$$Adhesion\ rate\ (\%) = (A_0 - A_1 - A_2)/A_0 \times 100\%.$$

Briefly, HCT-116 cells were detached, centrifuged, counted, and prepared into a final cell suspension of 2×10^5 cells/mL per group (A_0) and seeded onto the culture medium-dampened scaffolds in 24-well plates. Subsequently, the number of unattached cells in the culture medium was counted after 1, 3, and 6 h (A_1). Next, the scaffolds were taken out, the cells were eluted with 0.25% trypsin, and the number of cells that remained adherent was taken as A_2.

Cell proliferation in scaffold and the extracting liquid of scaffold

The proliferation of cells cultured on a 2D plate, SF/Cs (1: 1) scaffolds, and SF/Cs/Alg (1: 1: 1) scaffolds was determined using CCK-8. Briefly, 1 mL of cell suspension containing 5×10^4 cells was seeded on the prewetted scaffolds. Cell proliferation was checked on days 1, 3, and 5 following the manufacturer's protocol. Briefly, we added 20 µL of CCK-8 reagent to each well in the dark and the plates were incubated for 3 h. Subsequently, the plates were agitated for 15 min before removing the scaffolds and shifted to a 96-well plate to measure the absorbance at 450 nm. For cell proliferation in the extracting liquid of the scaffold, the scaffolds were placed into Dulbecco's modified Eagle medium (DMEM) complete culture medium and soaked for 3 d in a humidified incubator (37°C, 5% CO_2) to prepare the extracting liquid of the scaffold that was used for cell culture. Cell proliferation in the extracting liquid of the scaffold was detected using the CCK-8 kit as per the manufacturer's protocol.

Colony-forming assay and wound-healing assays of cells in the extracting liquid of scaffold

Colony-formation assay

A total of 1500 cells was seeded per 60-mm Petri dish and incubated using the extracting liquid of the scaffold for 12 d. Subsequently, the colonies were stained with crystal violet and counted (>50 cells under a microscope was the criterion to define a colony).

Wound-healing assays

Approximately 5×10^4 cells/well were plated and incubated using the extracting liquid of the scaffold in a 6-well plate. After overnight incubation, wounds were created by scratching the monolayer surface using a sterile 10-µL pipette tip. Cells were cultured in different kinds of serum-free media (DMEM complete culture medium, the extracting liquid of the SF/Cs [1: 1] scaffold, and the extracting liquid of the SF/Cs/Alg scaffold). The closure and gaps were measured using Image J software and the plates were photographed using an inverted microscope (Nikon ECLIPSE Ts2R).

Cell growth, microstructure, and ultrastructure in scaffolds and the extracting liquid of scaffolds

Cell proliferation analysis by green fluorescent protein (GFP)-labeled HCT116 cell imaging

pCDH-CMV-MCS-EF1-copGFP-Puro lentiviral expression vectors were purchased from Genesent (Hubei, China). Lentiviral vectors were produced in HEK 293T cells with packaging plasmids. The recombinant viral supernatants were harvested from HEK 293T cells and then used to infect HCT-116 cells in the presence of 8 µg/mL polybrene. After selection with puromycin-containing media for 72 h, HCT116 cells carrying GFP were cultured on 2D plates, SF/Cs (1: 1) scaffolds, and SF/Cs/Alg (1: 1: 1) scaffolds. The cells were observed under Nikon ECLIPSE Ts2R and photographs were taken on days 3 and 7.

4',6-Diamidino-2-phenylindole (DAPI) and DY-554-phalloidin staining

HCT-116 cells (5×10^5 cells) were cultured in the extracting liquid of a scaffold prepared in advance. For cytoskeleton staining, the cells were treated with 4% formaldehyde in PBS for 20 min, followed by dehydration with ethanol and permeabilization with 0.1% Triton X-100 for 5 min. The cytoskeleton was stained with 50 µg/mL DY-554-phalloidin–fluorescein isothiocyanate (FITC) solution for 30 min at room temperature and subsequently washed with PBS to remove unreacted DY-554-phalloidin conjugates. Nuclear staining was done with DAPI. The images were recorded under fluorescent microscope Leica DM2500.

Scanning electron microscopy

The culture medium was aspirated on days 3 and 7, and the scaffolds were rinsed with PBS three times. This was followed by the addition of 1 mL of 4% paraformaldehyde solution to fix the cells. Next, the plates were frozen at –20°C for 12 h before being placed in a –80°C freezer for 12 h. The plates were finally put into a freeze-drying machine for 48 h, and the morphology of cells on the scaffolds was imaged with a scanning electron microscope.

Hematoxylin and eosin (HE) staining

HE staining was performed to observe the growth state of cells in the scaffold over time and compare the morphology of the subcutaneous tumorigenesis model of nude mice with the morphology of multicellular spheroids in the scaffold under light microscopy (oil immersion). Two weeks after the HCT116 cells were inoculated under the skin, the nude mice were sacrificed and the tumor was excised. On days 3 and 7, SF/Cs (1: 1) and SF/Cs/Alg (1: 1: 1) scaffolds and excised tumors containing HCT-116 cells were fixed using 10% paraformaldehyde, embedded in paraffin, and cut into sections of 3-µm thickness. The sections were stained with HE and imaged under the oil-immersion lens using a Leica DM2500 microscope.
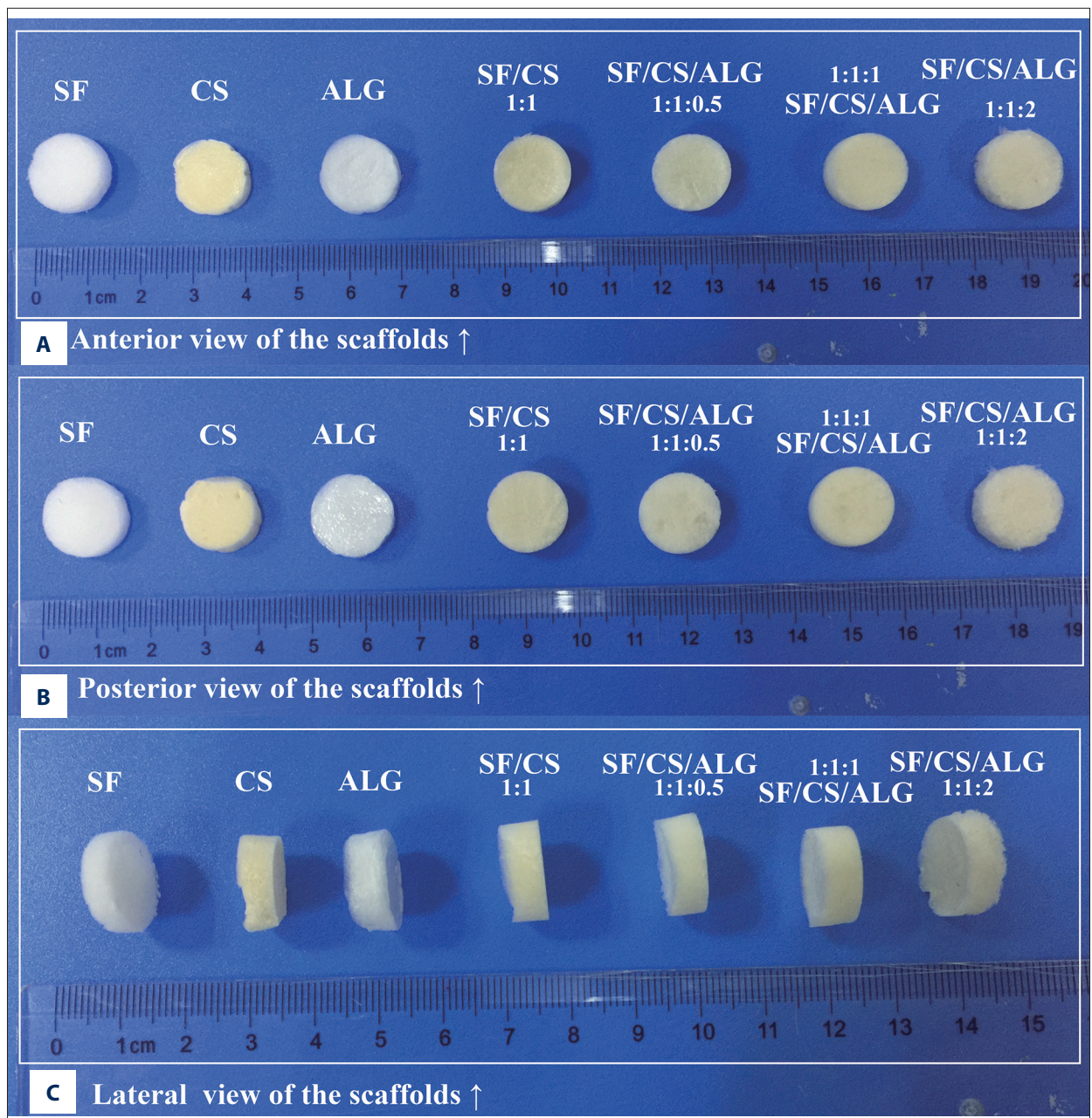
Figure 3. (**A–C**) Macroscopic appearance of silk fibroin (SF), chitosan (Cs), alginate (Alg), SF/Cs (1: 1), SF/Cs/Alg (1: 1: 0.5), SF/Cs/Alg (1: 1: 1), and SF/Cs/Alg (1: 1: 2) scaffolds is shown.

Statistical analysis

Graph Pad Prism 8 software (Graph Pad, San Diego, CA) was used to perform all statistical analyses. All experiments were performed in triplicate. Quantitative data were presented as the mean±standard deviation. Statistical significance was determined by analysis of variance and Student's *t* test. Differences were considered significant when *P*<0.05.

Results

Characterization of the 3D porous scaffolds

Macroscopic appearance

The macroscopic appearance of SF, Cs, Alg, SF/Cs (1: 1), SF/Cs/Alg (1: 1: 0.5), SF/Cs/Alg (1: 1: 1), and SF/Cs/Alg (1: 1: 2) scaffolds is shown in Figure 3. We observe that the SF and Alg scaffolds are pure white in color, whereas other scaffolds are
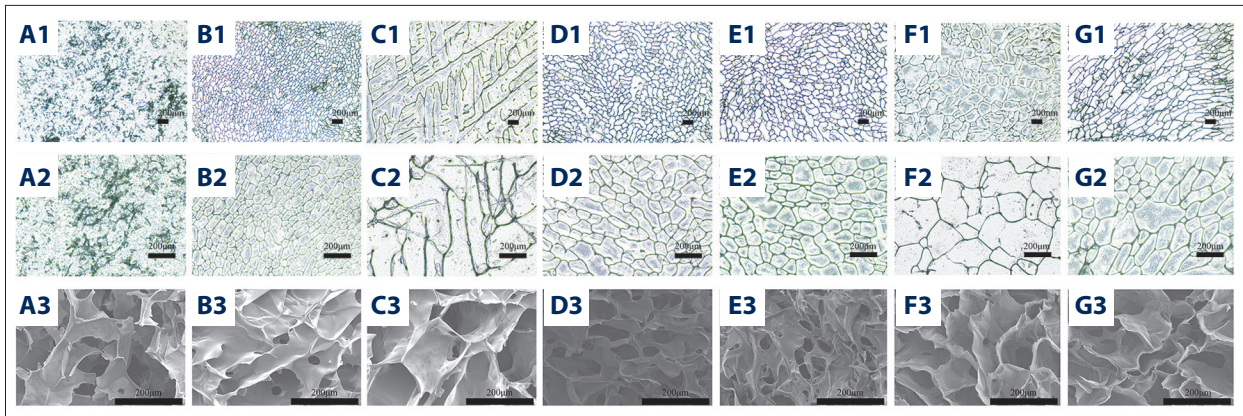
Figure 4. Optical microscope photographs (**A1–G1, A2–G2**) and scanning electron microscopy images (**A3–G3**) of the scaffolds made from silk fibroin (SF; **A1–A3**), chitosan (Cs; **B1–B3**), alginate (Alg; **C1–C3**), SF/Cs (1: 1) (**D1–D3**), SF/Cs/Alg (1: 1: 0.5) (**E1–E3**), SF/Cs/Alg (1: 1: 1), (**F1–F3**), and SF/Cs/Alg (1: 1: 2) (**G1–G3**), are presented.

Table 1. Frequency distribution of pore size of scaffolds made from silk fibroin (SF), chitosan (Cs), alginate (Alg), SF/Cs (1: 1), SF/Cs/Alg (1: 1: 0.5), SF/Cs/Alg (1: 1: 1), and SF/Cs/Alg (1: 1: 2). Image J was used to measure the cross-sectional area of pore for each group of scaffolds and the diameter of each pore was obtained by the formula: Area=$\pi d^2/4$, (d – diameter; NA – not available).

Pore-size distrbution	Groups						
	SF	Cs	Alg	SF/Cs (1: 1)	SF/Cs/Alg (1: 1: 0.5)	SF/Cs/Alg (1: 1: 1)	SF/Cs/Alg (1: 1: 2)
<50 μm (‰)	NA	13	NA	0	0	0	17
51–100 μm (‰)	NA	320	NA	13	10	0	85
101–200μm (‰)	NA	540	NA	204	485	125	193
201–300 μm (‰)	NA	120	NA	566	317	152	210
301–400 μm (‰)	NA	7	NA	164	149	241	223
401–500 μm (‰)	NA	0	NA	33	9	223	92
501–600 μm (‰)	NA	0	NA	7	20	107	91
601–700 μm (‰)	NA	0	NA	6	10	116	61
>701 μm (‰)	NA	0	NA	7	0	36	28
Mean value (μm)	NA	132	NA	255	221	400	319
Standard deviation	NA	56	NA	85	91	158	182
Coefficient of variation (%)	NA	42	NA	33	41	39	57

yellowish-white. The SF/Cs/Alg (1: 1: 1) scaffold is smoother and more symmetrical than other scaffolds.

Internal structure

We used an optical microscope and a scanning electron microscope to elucidate the internal structure of the scaffolds. As shown in Figure 4, all scaffolds have structures with porous network featuring different pore size and homogeneity and good connectivity between the pores except for the SF and

Alg scaffolds. The Cs alone, SF/Cs (1: 1), SF/Cs/Alg (1: 1: 0.5), SF/Cs/Alg (1: 1: 1), and SF/Cs/Alg (1: 1: 2) scaffolds have pores of different sizes and homogeneity. The SF/CS/Alg (1: 1: 1) scaffold has the largest pore size and good uniformity among all scaffolds (mean=400 μm, ranking first; coefficient of variation=39%, ranking second.) (Table 1).
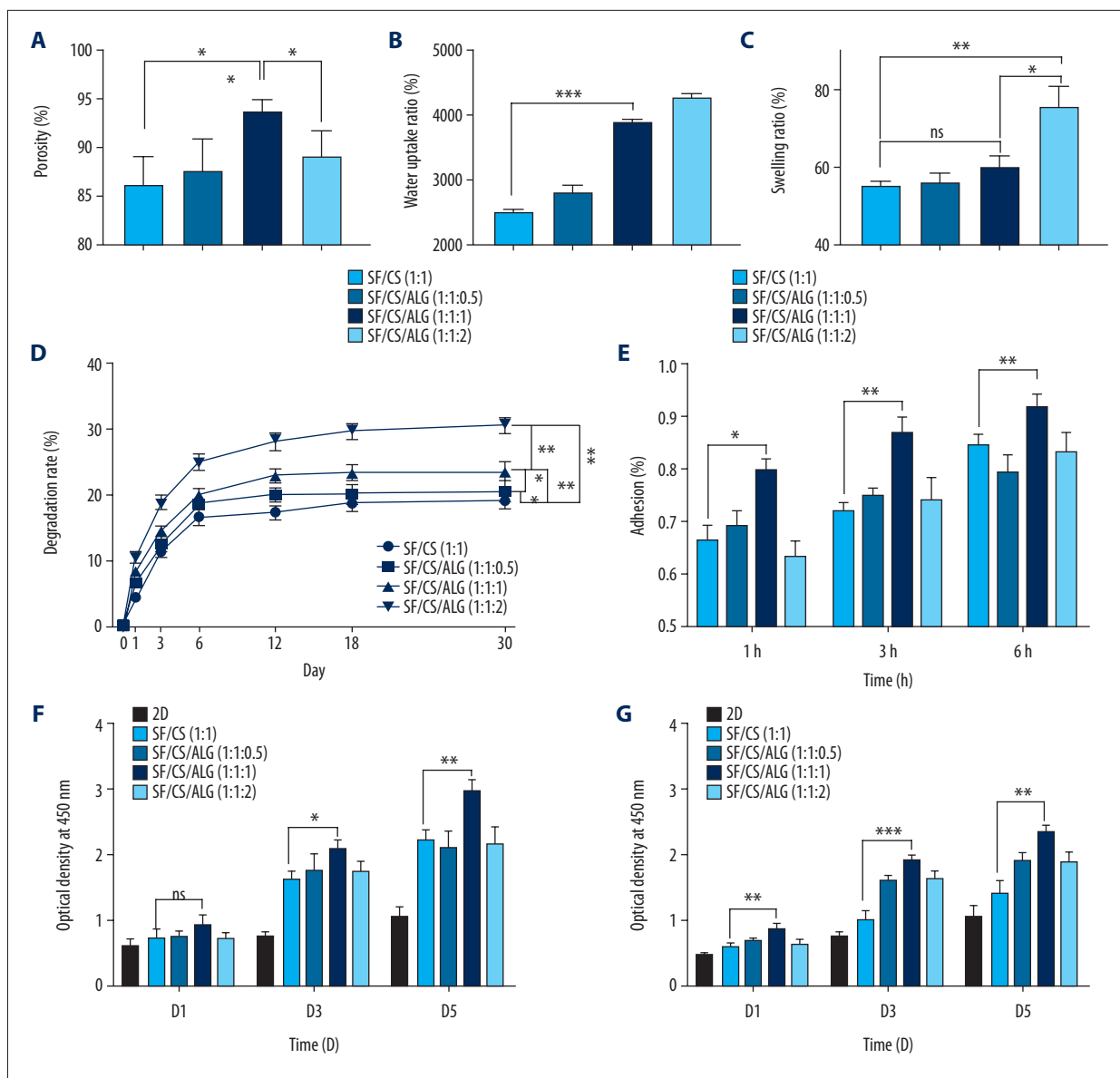
Figure 5. Results of porosity (**A**), water uptake rate (**B**), swelling rate (**C**) and degradation rate (**D**) of the scaffolds, and cell adhesion (**E**) and cell proliferation (**F, G**).

Physical and chemical properties

Porosity

All scaffolds have a porosity of greater than 83.09% (Figure 5A). Of all the scaffolds, the SF/Cs/Alg (1: 1: 1) scaffold has the highest porosity (93.73±1.12%), followed by the SF/Cs/Alg (1:41: 2) scaffold (88.96±2.70%). The porosity of the SF/CS scaffold and the SF/Cs/Alg (1: 1: 0.5) scaffold are 86.07±2.89% and 87.47±3.40%, respectively. Our results show that the difference between the porosity of SF/Cs (1: 1) and SF/Cs/Alg (1: 1: 1) scaffolds is statistically significant (*P*=0.013).

Water absorption rates

The water absorption rates of the scaffolds are illustrated in Figure 5B. Water uptake rates of all the scaffolds are above 2413.99% in deionized water. The SF/Cs/Alg (1: 1: 2) scaffold has the highest water uptake rate (5261.70±69.95%), followed by the SF/Cs/Alg (1: 1: 1) scaffold (3872.42±53.39%). On the other hand, the SF/Cs (1: 1) scaffold has the lowest water uptake rate (2473.38±60.00%). Our results show that the difference in the water absorption rates between SF/Cs (1: 1) and SF/Cs/Alg (1: 1: 1) scaffolds was statistically significant (*P*<0.001).

Swelling rates

The swelling rates of the samples are determined by placing them in buffers mimicking physiological fluids. Figure 5C describes the results from the swelling tests of the SF/Cs (1: 1), SF/Cs/Alg (1: 1: 0.5), SF/Cs/Alg (1: 1: 1), and SF/Cs/Alg (1: 1: 2) scaffolds at 37°C, where gels attained equilibrium swelling state at 24 h. We observe that the swelling rate of SF/Cs/Alg (1: 1: 2) scaffold is the highest among all the scaffolds, followed by SF/Cs/Alg (1: 1: 1), SF/Cs/Alg (1: 1: 0.5), and SF/Cs (1: 1). Our results show that the difference between the swelling rates of SF/Cs (1: 1) and SF/Cs/Alg (1: 1: 1) scaffolds was not statistically significant (P=0.071).

Degradation rates

The degradation rates of the scaffolds immersed in the culture medium are shown in Figure 5D. The addition of Alg enhanced the degradation properties of scaffolds, and the degree of enhancement was positively correlated with the amount of Alg added. The SF/Cs/Alg (1: 1: 2) scaffold has the highest degradation rate, followed by that of SF/Cs/Alg (1: 1: 1) scaffold. The SF/Cs (1: 1) scaffold has minimum degradation properties. Statistical analysis shows that pairwise comparisons among all groups present statistical differences (P<0.05). All four groups of scaffolds have different degrees of degradation within 30 d, but the general trend is similar. The sixth day is the inflection point; the first 6 d is a rapid degradation period; after 6 d is a slow degradation period; day 18 to day 30 is the plateau period.

Cell incorporation into scaffolds

Cell adhesion in scaffolds

Analysis of cell adhesion on the scaffold was performed by cell counting using a cell counting board at 1, 3, and 6 h after cell inoculation on the prewetted scaffolds. The cell adhesion rates are presented in Figure 5E, showing that the SF/Cs/Alg (1: 1: 1) scaffold has the highest cell adhesion rate (79.96±1.77% at 1 h to 91.96±2.43% at 6 h), followed by that of the SF/Cs (1: 1) scaffold (66.46±2.51% at 1 h to 84.49±2.33% at 6 h). The SF/Cs/Alg (1: 1: 1) scaffold shows significantly higher cell adhesion (P=0.0016, 0.0010, and 0.0185 for 1, 3, and 6 h, respectively).

Cell proliferation in scaffold and the extracting liquid of scaffold

We used a commercially available CCK-8 kit to measure cell proliferation on the scaffolds (Figure 5F) and the extracting liquid of the scaffold (Figure 5G). Our results show that the highest number of cells proliferated on the SF/Cs/Alg (1: 1: 1) scaffold at all time points. From the statistical results we know that the cell proliferation shows no significant difference between the two scaffolds on day 1 (P=0.143), whereas significantly higher cell proliferation is observed on the triple scaffold on day 3 (P=0.0075) and day 5 (P=0.0044). Results from cell proliferation in the extracting liquid of the scaffold show that the triple scaffold registered a higher cell proliferation (P=0.0032 at day 1, 0.0003 at day 3, and 0.0012 at day 5).

Colony-forming assay and wound-healing assays of cells in the extracting liquid of scaffold

To investigate whether the extracting liquid of the scaffold facilitated the migration, population dependence, and proliferation of HCT-116 cells, we performed a wound-healing assay (Figure 6A1–A3, B1–B3, C1–C3) and colony-forming assay (Figure 6D1–D3). We observed that the cell mobility is significantly increased in the extracting liquid of the scaffold compared with the control (Figure 6E, 6F). At 96 h, the wound-healing percentage of the SF/Cs/Alg (1: 1: 1) group (46.44±1.17%) is greater than that of the SF/Cs (1: 1) group (63.60±1.15%) (P=0.00005). At 192 h, the wound-healing percentage of SF/Cs/Alg (1: 1: 1) (69.42±1.13%) is greater than that of SF/Cs (1: 1) (78.75±1.29%) (P=0.0007). Similarly, the results from the colony-forming assay demonstrated considerable augmentation in colony-forming efficiency in the extracting liquid of the scaffold when compared with the control (Figure 6G). The cloning efficiency of SF/Cs/Alg (1: 1: 1) is greater than that of SF/Cs (1: 1) (P=0.005).

Cell growth, microstructure, and ultrastructure in scaffolds and the extracting liquid of scaffolds

Cell proliferation analysis by GFP-labeled HCT116 cells imaging

On the basis of our experimental results that the scaffolds may be closely associated with the enhanced proliferation of cancer cells, we sought to validate the findings by monitoring the cell growth of HCT-116 cell line transfected with pCDH-CMV-MCS-EF1-copGFP-Puro lentivirus. Cell growth is monitored by measuring the GFP expression over a 7-d period. The proliferation of HCT-116 cells transfected with pCDH-CMV-MCS-EF1-copGFP-Puro lentivirus is significantly higher than the control cells, and the difference became prominent in a time-dependent manner. Compared with the 2D plate, more cells cultured in the scaffold exhibited spheroids. The numbers and dimensions of spheroids in the SF/Cs/Alg (1: 1: 1) scaffolds are higher than those in the SF/Cs (1: 1) scaffolds (Figure 7).

DAPI and DY-554-phalloidin staining

We used DAPI to stain the cell nuclei to confirm cell division, and it is evident that there is statistically significant difference in the number of cells per field among the three groups (2D,
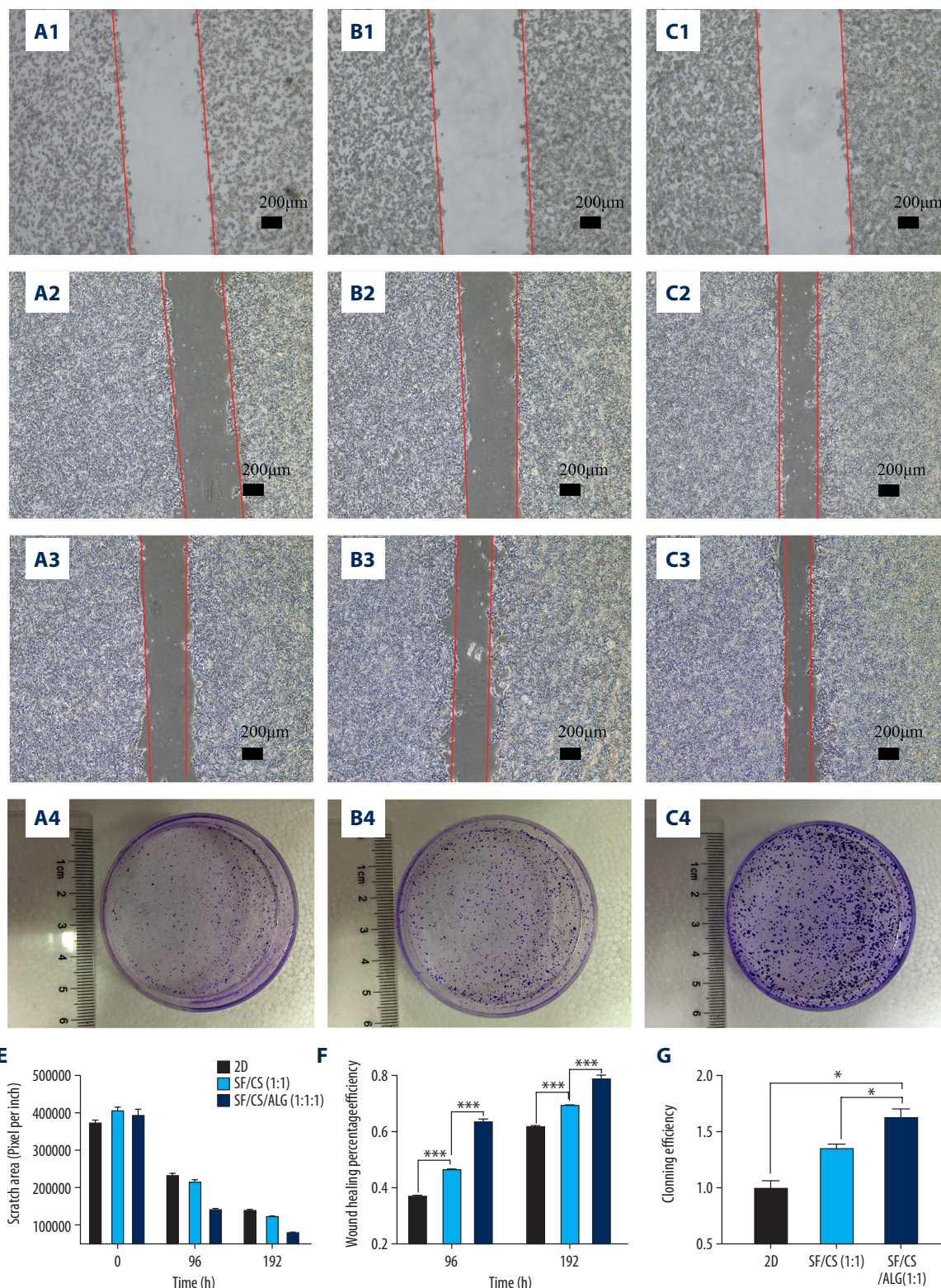
Figure 6. Results of wound-healing assays (**A1–A3, B1–B3, C1–C3, E, F**) and colony-forming assay (**D1–D3, G**) of cells in the extracting liquid of the scaffold are represented.
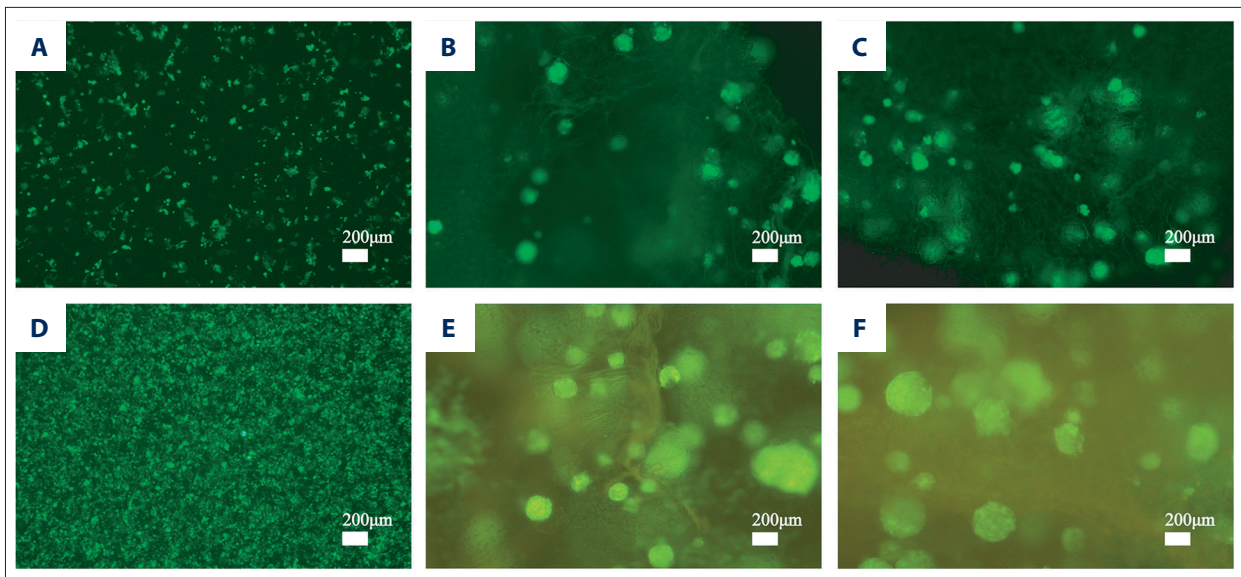
Figure 7. Cell proliferation analyses are accomplished by green fluorescent protein (GFP)-labeled HCT116 cell imaging. HCT-116 cells transfected with pCDH-CMV-MCS-EF1-copGFP-Puro lentivirus (5×10^9 transduction units/mL) were cultured in the two-dimensional (2D) plate, silk fibroin (SF)/chitosan (Cs) (1: 1) scaffolds, and SF/Cs/alginate (Alg) (1: 1: 1) scaffolds. The scaffolds and the cells are observed under Nikon ECLIPSE Ts2R microscope and images are taken on day 3 (**A–C**) and day 7 (**D–F**). 2D group (**A, D**), SF/Cs (1: 1) group (**B, E**), SF/Cs/Alg (1: 1: 1) group (**C, F**).

SF/Cs [1: 1], SF/Cs/Alg [1: 1: 1]) at all time points ($P<0.001$) (Figure 8A1, A2; B1, B2; C1, C2). SF/Cs/Alg (1: 1: 1) has the highest cell proliferation capacity.

The cytoskeleton plays an important role in maintaining cell morphology, movement, and cell division. To observe the organization of the cytoskeleton, we used DY-554-phalloidin-FITC to stain actin filaments; the optical microscope Leica DM2500 was used to image the cells. Our results show that cells in the 2D group are rich in actin, with a decreasing and regular organization from the nuclear periphery to the membrane. However, our findings are consistent with an earlier report that shows that after treatment with the extracting liquid of the scaffold, actin organization changed dramatically, with an abundant but disordered local concentration in the cytoplasm, a contractile ring around the nucleus, and a contraction ring at the location of the cell mitosis groove. Consistent with these findings, we also observe that the cells grown in 2D culture are mainly long and spindle shaped, whereas the cells grown on the scaffold of SF/Cs (1: 1) and SF/Cs/Alg (1: 1: 1) are mainly round, indicating cells undergoing cell division. More cells in the dividing phase are observed in the extracting liquid of the SF/Cs/Alg (1: 1: 1) scaffold (Figure 8D1, D2; E1, E2; F1, F2).

Scanning electron microscope

The SEM images showing the morphology of the cells on the scaffolds are presented in Figure 9. We observe that the diameter of the channel in SF/Cs/Alg (1: 1: 1) is larger than that

in SF/Cs (1: 1), which provides a broader space for cell division and proliferation. More cells proliferated on the Alg-containing scaffolds; the SF/Cs/Alg (1: 1: 1) scaffold supported a greater cell proliferation under the same conditions than the SF/Cs (1: 1) scaffold. The cellular morphology in the 3D scaffolds (SF/Cs/Alg [1: 1: 1] and SF/Cs [1: 1]) is quite different from that in the common culture dish. In the 3D scaffold, the cells do not adhere to the scaffold completely and maintained their shape as *in vivo*. Moreover, though the cells grew in number over time, they did not spread over the internal surface of scaffolds. It is clear from these results that the 3D scaffolds provide a better culture system than a regular culture dish. We also observed that more cells proliferated on the Alg-containing scaffolds; the SF/Cs/Alg (1: 1: 1) scaffold supported a greater cell proliferation under the same conditions.

HE staining

The images of HE-stained scaffolds are shown in Figure 10. Consistent with our SEM results, these results show that the diameter of the channel in SF/Cs/Alg (1: 1: 1) is larger than that in SF/Cs (1: 1), which provides a broader space for cell division and proliferation. More cells proliferated on the Alg-containing scaffolds; the SF/Cs/Alg (1: 1: 1) scaffold supported a greater cell proliferation under the same conditions than the SF/Cs (1: 1) scaffold. However, the cells on the scaffold of SF/Cs (1: 1) and SF/Cs/Alg (1: 1: 1) tend to be spherical and cling to each other rather spreading out, which is more obvious in the SF/Cs/Alg (1: 1: 1) group than in the SF/Cs (1: 1)
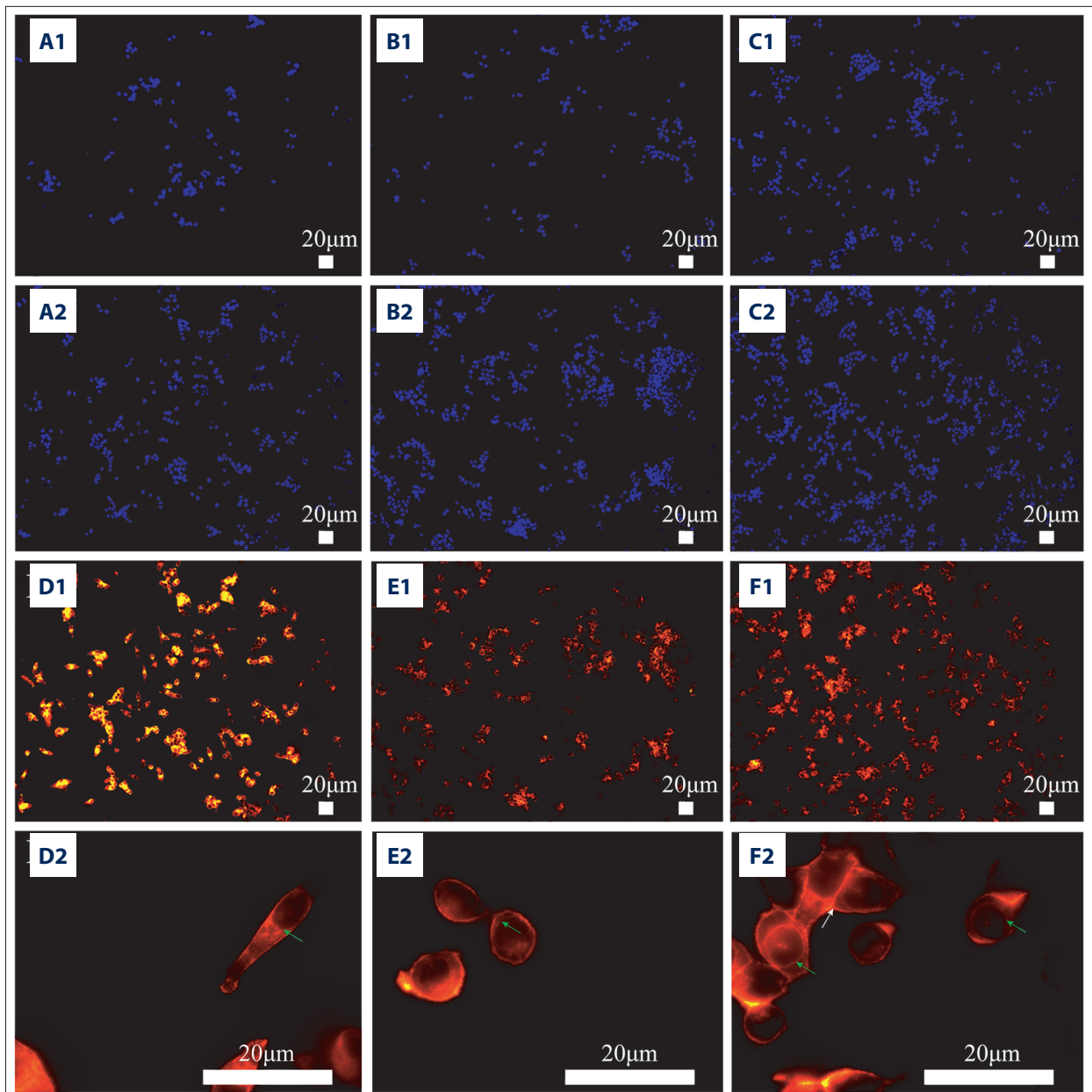
Figure 8. Fluorescence staining of actin in HCT-116 cells cultured in the extracting liquid of scaffold. F-Actin is marked with fluorescein isothiocyanate (FITC)-DY-554-phalloidin (red). Nuclear counterstain with 4',6-diamidino-2-phenylindole (DAPI; blue). Two-dimensional (2D) culture system on day 3 (**A1**), silk fibroin (SF)/chitosan (Cs) (1: 1) scaffold on day 3 (**B1**), SF/Cs/alginate (Alg) (1: 1: 1) scaffold on day 3 (**C1**), 2D culture system on day 7 (**A2, D1, D2**), SF/Cs (1: 1) scaffold on day 7 (**B2, E1, E2**), SF/Cs/Alg (1: 1: 1) scaffold on day 7 (**C2, F1, F2**). The green arrow indicates the contractile ring around the nucleus, and the white arrow indicates the contraction ring at the location of the cell mitosis groove.

group. The multicellular globules formed on the scaffold are morphologically similar to the subcutaneous tumor seen in nude mice. In tumors and multicellular spheroids, cells maintain close contact with each other.

Discussion

The classical 2D cell cultures provide researchers a convenient *in vitro* platform to carry out cancer research. However, cells cultured on flat Petri dish surfaces do not ideally represent the cell–ECM and cell–cell interactions or tumor architecture *in vivo*, and display a dramatically reduced malignant
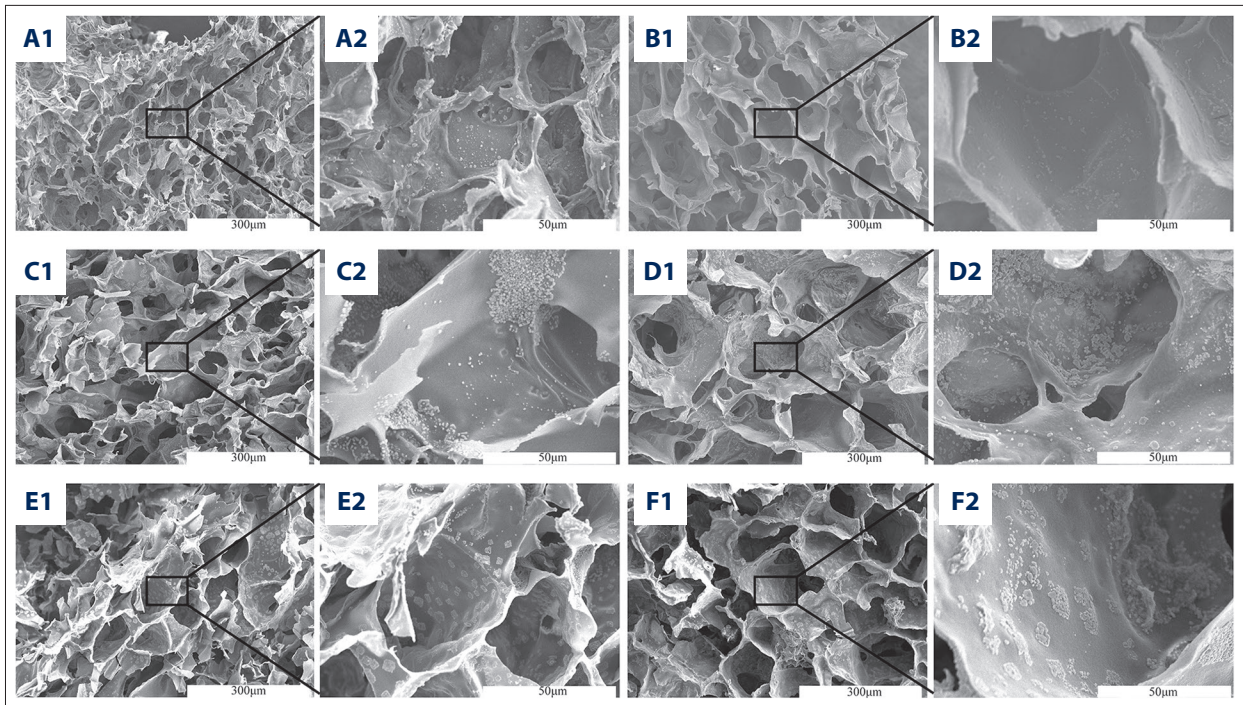
Figure 9. Scanning electron microscopy images of cell morphology on the scaffolds. Silk fibroin (SF)/chitosan (Cs) (1: 1) scaffold on day 1 (**A1, A2**), SF/Cs (1: 1) scaffold on day 3 (**C1, C2**), SF/Cs (1: 1) scaffold on day 7 (**E1, E2**), SF/Cs/alginate (Alg) (1: 1: 1) scaffold on day 1 (**B1, B2**), SF/Cs/Alg (1: 1: 1) scaffold on day 3 (**D1, D2**), SF/Cs/Alg (1: 1: 1) scaffold on day 7 (**F1, F2**).

phenotype [3]. SF, Cs, and Alg have been instrumental in propelling the development of a 3D cell culture system to generate scaffolds with desirable properties. Compared with the pure SF scaffold of *B. mori*, the blend scaffolds differ in morphology, porosity, elasticity, swelling behavior, and biochemical composition. Previously, SF/Cs (1: 1) was proven to be a potential biomaterial for generating scaffolds for cancer therapy [23]. Coincidentally, a recent study suggested that the SF/Cs (1: 1) scaffolds can improve cell growth as a 3D cell culture platform for prostate cancer research compared with matrices based on pure biomaterials or synthetic polymers [24]. However, the results from our preliminary experiment have shown that the SF/Cs (1: 1) scaffold has poor water absorption as well as low degradation and cell adhesion rates, thereby restricting their applications in the 3D cell culture. Alg is also known as Alg gel, a long-chain polymer consisting of (1→4)-alpha-cross-linked guluronic acid and (1→4)-beta-cross-linked d-mannituronic acid with a relative molecular mass of about 10^6. Alg is found mainly in the cell walls and intercellular mucilage of brown algae. Alg is widely used in medical swabs and surgical dressings because of its good water absorption and plasticity. In addition, because of its excellent adhesion properties, it is also used as a solid-phase support vector for cells in laboratory applications. On the basis of the above advantages, we tried to add Alg into the SF/Cs (1: 1) blend to improve the characteristics of the SF/Cs (1: 1) scaffold and make it more suitable for cell culture. Although the internal structure of the SF/Cs (1: 1)

scaffold is more complex than that of the 2D cell culture system, it is still simpler than the tumor cell microenvironment *in vivo*, especially in terms of chemical composition. The addition of Alg can increase the chemical composition complexity of the scaffold and make it more closely simulate the microenvironment of growing cells. We hypothesized that the triple biomaterial composite scaffolds would have better characteristic features and improved performance than the composite scaffolds made from two biomaterials. Interestingly, our results show that although HCT-116 cell spheroids in all four kinds of 3D scaffolds (SF/Cs [1: 1], SF/Cs/Alg [1: 1: 0.5], SF/Cs/Alg [1: 1: 1], and SF/Cs/Alg [1: 1: 2]) show tumorlike morphological characteristics seen *in vivo*, the cells grown in the 3D scaffold made from SF/Cs/Alg (1: 1: 1) are more likely to aggregate into spheres and exhibit highly malignant behavior, a characteristic feature of tumor cells *in vivo*.

SF, Cs, and Alg are thought to interact with each other via OH– and COO– groups, resulting in the formation of hydrogen bonds and electrostatic interactions that improve the tensile strength of the polymers made from them. The addition of Alg to the SF/CS (1: 1) blend scaffold enhanced its overall porosity and average pore diameter. Adequate pore size and porosity provide physical space, improved oxygen and nutrient availability to cells, and facilitate efficient metabolic waste removal, thereby remarkably influencing attachment, proliferation, migration, distribution, differentiation, mitosis, and

metabolic activity of the cells [25]. An optimal scaffold pore size has been reported to depend on the specific cell type [26]. In our study, the SF/Cs/Alg (1: 1: 1) scaffold with the biggest average pore size (~400 μm) is best suited for HCT-116 cell culture and growth. Scaffolds with high porosity facilitate enhanced cellular infiltration and mechanical interlocking [27]. In our study, SF/Cs/Alg (1: 1: 1) scaffold has the highest porosity (93.73±1.12%) and supported the maximum cell growth.

A higher water uptake ratio is preferable for the cells to infiltrate the scaffold. A lower swelling ratio helps the scaffold to maintain its structural stability. In our case, the increase in the proportion of Alg polymer led to a gradual increase in the water uptake ratio, swelling ratio, and degradation rate. Our results show that the SF/Cs/Alg (1: 1: 1) scaffold has a high water absorption rate (3872.42±53.39%), low swelling rate (60.18±3.05%), and appropriate degradation rate.
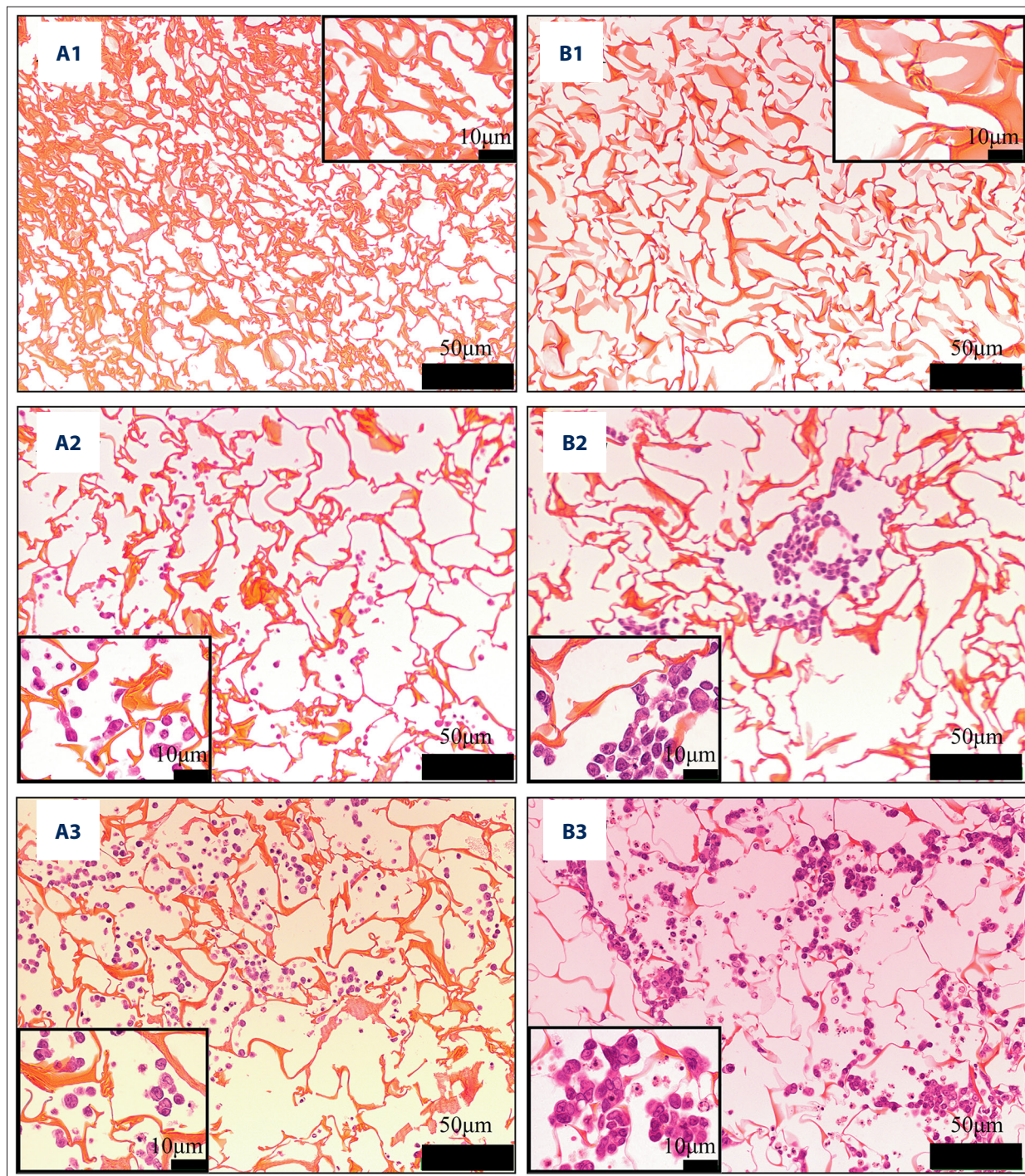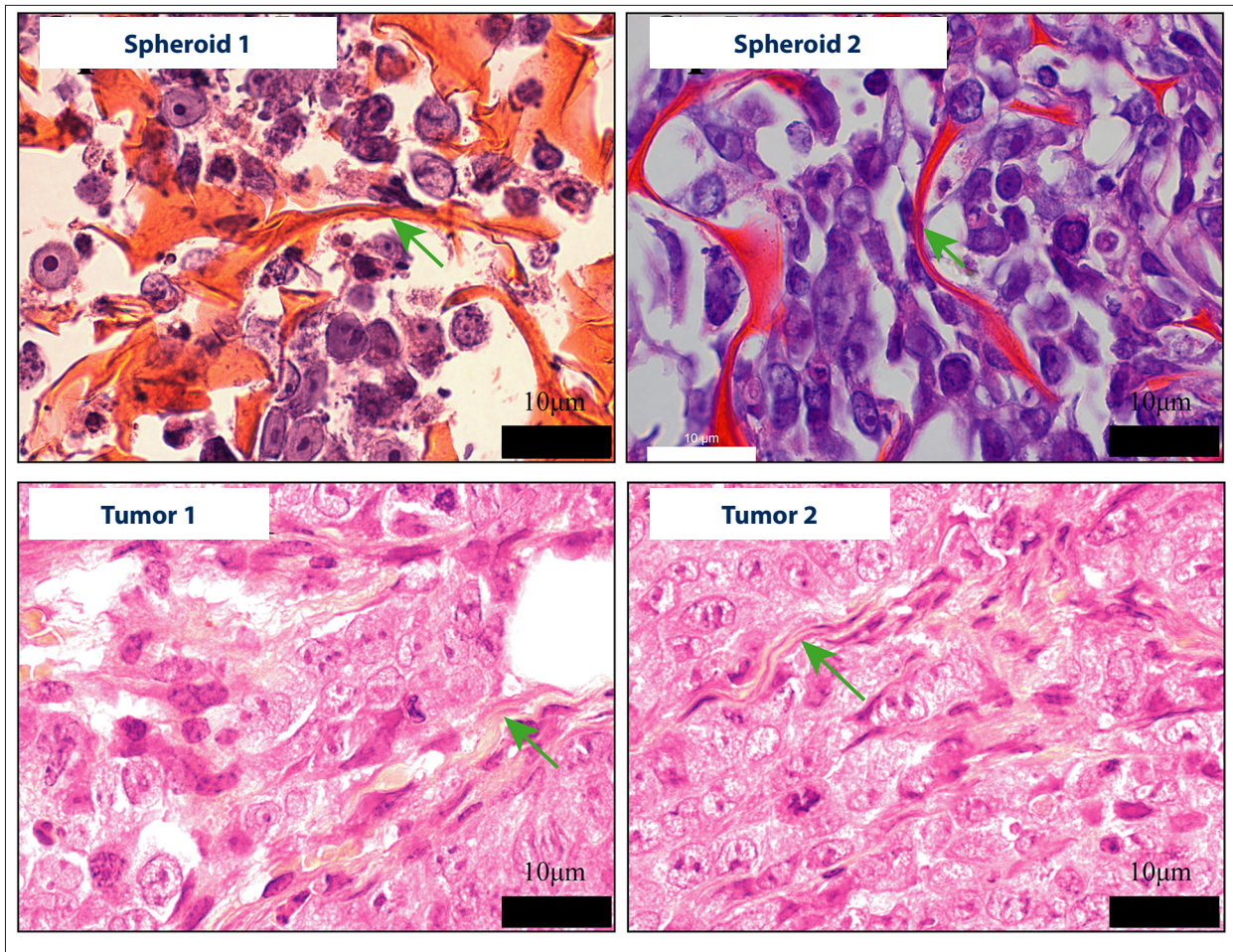
Figure 10. Images of hematoxylin and eosin staining of scaffold. Silk fibroin (SF)/chitosan (Cs) (1: 1) scaffold without cells (**A1**), SF/Cs/alginate (Alg) (1: 1: 1) scaffold without cells (**B1**), SF/Cs (1: 1) scaffold with cells on day 3 (**A2**), SF/Cs/Alg (1: 1: 1) scaffold with cells on day 3 (**B2**), SF/Cs (1: 1) scaffold with cells on day 7 (**A3**), SF/Cs/Alg (1: 1: 1) scaffold with cells on day 7 (**B3**). Spheroids formed in the SF/Cs (1: 1) scaffold are observed under oil lens of Leica DM2500 (**spheroid 1**). Spheroids formed in the SF/Cs/Alg (1: 1: 1) scaffold are observed under oil lens of Leica DM2500 (**spheroid 2**). Tumor formed subcutaneously in nude mice after inoculation with HCT-116 cells, observed under oil lens of Leica DM2500 (**tumor 1, 2**). Green arrows indicate the fiber band.

Our results from the characterization of these scaffolds show that the highest cell adhesion and proliferation rates are observed for cells on SF/Cs/Alg (1: 1: 1), and these results are supported by the cell growth and morphological features shown by SEM. The combined results from the biological characterization indicated that the SF/Cs/Alg (1: 1: 1) scaffold may be the best one for *in vitro* research on CC cells. Results from the staining of scaffolds and cells show that cells maintained their *in vivo* morphology in the 3D scaffolds. During their spread in new tissue *in vivo* or in a new environment *in vitro*, cells undergo significant changes in their architecture, protein expression, and mechanical properties. Cells can adapt to such transitions because of their plasticity, and cytoskeleton rearrangement plays a significant role in it. We further investigated the facilitating effect of SF/Cs/Alg (1: 1: 1) toward cellular

cytoskeleton realignment by staining with DY-554-phalloidin-FITC. It is well known that the cytoskeleton can be remodeled during the cellular processes such as movement, migration, adhesion, and proliferation [28]. The cytoskeletal network plays a vital role in maintaining cell morphology [29], and it has been reported that the correct cytoskeletal arrangement is an important requirement for the smooth progression of the cell cycle [30]. Our results show that the cells on the SF/Cs/Alg (1: 1: 1) scaffold grew the fastest, followed by the SF/Cs (1: 1) group, and slowest in the 2D group. The cells on the SF/Cs/Alg (1: 1: 1) scaffolds and SF/Cs (1: 1) scaffolds are round or nearly round, whereas most of the cells in the 2D group are long fusiform, which could be explained by the reconstruction of the cell skeleton and the state of cell mitosis and migration. SF/Cs (1: 1) and SF/Cs/Alg (1: 1: 1) scaffolds both favor cytoskeletal

rearrangement by inducing the formation of contractile rings around the nucleus and at the mitosis groove compared with 2D cell culture, which is more common in SF/CS/Alg (1: 1: 1) scaffolds. The contraction bands and contraction rings are also more distinct for cells planted in SF/Cs/Alg (1: 1: 1) scaffolds. To verify and interpret our results, we reviewed additional published literature. The results show that these rings can cause deformation of the nuclei in the spreading cells [31,32]. The presence of ringlike cytoskeletal structures is commonly seen in cells that have undergone mitosis. The ringlike structures composed of the intermediate cytoskeleton and their nuclear invaginations have been previously reported in different cancer cell lines, especially in undifferentiated human pancreatic carcinoma cells [33].

We observe that, unlike the 2D monolayer model, HCT-116 cells implanted on 3D scaffolds tend to aggregate into multicellular spheroids. These 3D multicellular aggregates (spheroids) recapitulate the natural tumor microenvironment and thus have emerged as an important alternative for cancer research [34]. Our findings show that the SF/Cs/Alg (1: 1: 1) scaffold supported the growth of larger spheroids than that seen in SF/Cs (1: 1). There is increasing evidence that multicellular structures respond to mechanical cues, such as the confinement and compression exerted by the surrounding environment. An earlier study compared the response of multicellular spheroids and individual cells to the same osmotic perturbation, and their results show a more significant decrease in the volume of multicellular spheroids than the individual cells when subjected to the same pressure [36]. In light of these results and on the basis of our observation, we opine that SF/Cs/Alg (1: 1: 1) provides a broader surrounding environment for HCT-116 cells to grow and thus facilitates the formation of larger spheroids. Many techniques have been reported to construct 3D spheroids, among which the formation of substrate-derived spheroids and the mechanism of their formation is unique [36]. Our results, on the basis of formation of biomaterial substrate-mediated multicellular spheroids, are a testimony to this observation.

Though our study provides some interesting insights into the development and potential of composite scaffolds synthesized from compatible biopolymers, many questions remain unanswered. For instance, the underlying mechanism of our observations remains unknown. Although our SF/Cs/Alg (1: 1: 1) scaffold shows the best results related to cell adhesion, proliferation, migration, and spheroid formation, it ranked second in water absorption and degradation rate. We could not draw a conclusion regarding the relationships among water absorption rate, degradation rate, and cell growth. Last but not least, although our results show the best results with the SF/Cs/Alg (1: 1: 1) scaffold, which has an average pore size of 400 μm, we are unable to draw a conclusion about the optimal pore size. This warrants further research to elucidate the underlying mechanism of these scaffolds supporting cell growth and proliferation, the best pore size of composite scaffolds to support the same, and to validate these findings before these 3D models can be optimized and made available to clinical and basic science researchers worldwide.

Conclusions

Our comparative study of HCT-116 cell culture using three different scaffolds (2D, 3D SF/Cs [1: 1] scaffold, and 3D SF/Cs/Alg [1: 1: 1] triple scaffold) show that the biological behavior of CC cells varied with the types of materials used. Our results show that the SF/Cs/Alg (1: 1: 1) scaffold holds potential for developing into a promising experimental model for CC cell culture experiments and mimicking the 3D cell growth environment *in vivo*.

Availability of data and materials

The data sets used and analyzed during the current study are available from the corresponding author on reasonable request.

Acknowledgment

Conflicts of interest

None.

References:

1. Bray F, Ferlay J, Soerjomataram I et al: Global cancer statistics 2018: GLOBOCAN estimates of incidence and mortality worldwide for 36 cancers in 185 countries. Cancer J Clin, 2018; 68(6): 394–424

2. Brody H: Colorectal cancer. Nature, 2015; 521: S1

3. Smalley KS, Lioni M, Herlyn M: Life isn't flat: Taking cancer biology to the next dimension. In Vitro Cell Dev Biol Anim, 2006; 42(8–9): 242–47

4. Ravi M, Paramesh V, Kaviya SR et al: 3D cell culture systems: Advantages and applications. J Cell Physiol, 2015; 230(1): 16–26

5. Jensen C, Teng Y: Is it time to start transitioning from 2D to 3D cell culture? Front Mol Biosci, 2020; 7: 33

6. Ravi M, Ramesh A, Pattabhi A: Contributions of 3D cell cultures for cancer research. J Cell Physiol, 2017; 232(10): 2679–97

7. Salerno A, Zeppetelli S, Di Maio E et al: Processing/structure/property relationship of multi-scaled PCL and PCL-HA composite scaffolds prepared via gas foaming and NaCl reverse templating. Biotechnol Bioeng, 2011; 108(4): 963–76

8. Scaglione S, Lazzarini E, Ilengo C, Quarto R: A composite material model for improved bone formation. J Tissue Eng Regen Med, 2010; 4(7): 505–13

9. Du M, Gu J, Wang J et al: Silk fibroin/poly(L-lactic acid-co-epsilon-caprolactone) electrospun nanofibrous scaffolds exert a protective effect following myocardial infarction. Exp Ther Med, 2019; 17(5): 3989–98

10. Li J, Wang Q, Gu Y et al: Production of composite scaffold containing silk fibroin, chitosan, and gelatin for 3D cell culture and bone tissue regeneration. Med Sci Monit, 2017; 23: 5311–20

11. Keane TJ, Badylak SF: The host response to allogeneic and xenogeneic biological scaffold materials. J Tissue Eng Regen Med, 2015; 9(5): 504–11

12. Reddy R, Reddy N: Biomimetic approaches for tissue engineering. J Biomater Sci, 2018; 29(14): 1667–85

13. Chomchalao P, Pongcharoen S, Sutheerawattananonda M, Tiyaboonchai W: Fibroin and fibroin blended three-dimensional scaffolds for rat chondrocyte culture. Biomed Eng Online, 2013; 12(1): 28

14. Patrulea V, Ostafe V, Borchard G, Jordan O: Chitosan as a starting material for wound healing applications. Eur J Pharm Biopharm, 2015; 97(Pt B): 417–26

15. Augst AD, Kong HJ, Mooney DJ: Alginate hydrogels as biomaterials. Macromol Biosci, 2006; 6(8): 623–33

16. Ghosh M, Halperin-Sternfeld M, Adler-Abramovich L: Bio mimicking of extracellular matrix. Adv Exp Med Biol, 2019; 1174: 371–99

17. Gu Y, Zhu J, Xue C et al: Chitosan/silk fibroin-based, Schwann cell-derived extracellular matrix-modified scaffolds for bridging rat sciatic nerve gaps. Biomaterials, 2014; 35(7): 2253–63

18. Bhardwaj N, Nguyen QT, Chen AC et al: Potential of 3-D tissue constructs engineered from bovine chondrocytes/silk fibroin-chitosan for *in vitro* cartilage tissue engineering. Biomaterials, 2011; 32(25): 5773–81

19. Rios CN, Skoracki RJ, Miller MJ et al: *In vivo* bone formation in silk fibroin and chitosan blend scaffolds via ectopically grafted periosteum as a cell source: A pilot study. Tissue Eng Part A, 2009; 15(9): 2717–25

20. Muzzarelli R, El Mehtedi M, Bottegoni C et al: Genipin-crosslinked chitosan gels and scaffolds for tissue engineering and regeneration of cartilage and bone. Mar Drugs, 2015; 13(12): 7314–38

21. Li Z, Leung M, Hopper R et al: Feeder-free self-renewal of human embryonic stem cells in 3D porous natural polymer scaffolds. Biomaterials, 2010; 31(3): 404–12

22. Serra IR, Fradique R, Vallejo MCS et al: Production and characterization of chitosan/gelatin/β-TCP scaffolds for improved bone tissue regeneration. Mater Sci Eng C, 2015; 55: 592–604

23. Gupta V, Aseh A, Ríos CN et al: Fabrication and characterization of silk fibroin-derived curcumin nanoparticles for cancer therapy. Int J Nanomedicine, 2009; 4: 115–22

24. Backer A, Erhardt O, Wietbrock L et al: Silk scaffolds connected with different naturally occurring biomaterials for prostate cancer cell cultivation in 3D. Biopolymers, 2017; 107(2): 70–79

25. Nava MM, Draghi L, Giordano C, Pietrabissa R: The effect of scaffold pore size in cartilage tissue engineering. J Appl Biomater Funct Mater, 2016; 14(3): e223–29

26. Murphy CM, Duffy GP, Schindeler A, O'Brien FJ: Effect of collagen-glycosaminoglycan scaffold pore size on matrix mineralization and cellular behavior in different cell types. J Biomed Mater Res A, 2016; 104(1): 291–304

27. Ionescu LC, Mauck RL: Porosity and cell preseeding influence electrospun scaffold maturation and meniscus integration *in vitro*. Tissue Eng Part A, 2013; 19(3–4): 538–47

28. Jin H, Pi J, Huang X et al: BMP2 promotes migration and invasion of breast cancer cells via cytoskeletal reorganization and adhesion decrease: an AFM investigation. Appl Microbiol Biotechnol, 2012; 93(4): 1715–23

29. Ma L, Song B, Jin H et al: Cinobufacini induced MDA-MB-231 cell apoptosis-associated cell cycle arrest and cytoskeleton function. Bioorg Med Chem Lett, 2012; 22(3): 1459–63

30. Jiang J, Jin H, Liu L et al: Curcumin disturbed cell-cycle distribution of HepG2 cells via cytoskeletal arrangement. Scanning, 2013; 35(4): 253–60

31. Strube F, Infanger M, Wehland M et al: Alteration of cytoskeleton morphology and gene expression in human breast cancer cells under simulated microgravity. Cell J, 2020; 22(1): 106–14

32. Terriac E, Schütz S, Lautenschläger F: Vimentin intermediate filament rings deform the nucleus during the first steps of adhesion. Front Cell Dev Biol, 2019; 7: 106

33. Kamei H: Relationship of nuclear invaginations to perinuclear rings composed of intermediate filaments in MIA PaCa-2 and some other cells. Cell Struct Funct, 1994; 19(3): 123–32

34. Hirschhaeuser F, Menne H, Dittfeld C et al: Multicellular tumor spheroids: An underestimated tool is catching up again. J Biotechnol, 2010; 148(1): 3–15

35. Monnier S, Delarue M, Brunel B et al: Effect of an osmotic stress on multicellular aggregates. Methods, 2016; 94: 114–19

36. McMahon KM, Volpato M, Chi HY et al: Characterization of changes in the proteome in different regions of 3D multicell tumor spheroids. J Proteome Res, 2012; 11(5): 2863–75